Original Research Article: full paper

(2024), «EUREKA: Physics and Engineering»
Number 4

STUDYING THE INFLUENCE OF ENGINE SPEED ON THE ENTIRE PROCESS OF SPAN-LOWERING OF THE HEAVY MECHANIZED BRIDGE

Duong Van Le
Institute of Vehicle and Energy Engineering[1]

Thang Duc Tran✉
Institute of Vehicle and Energy Engineering[1]
thangdt135@mta.edu.vn

Quyen Manh Dao[2]

Dat Van Chu
Institute of Vehicle and Energy Engineering[1]

[1]*Le Quy Don Technical University*
236 Hoang Quoc Viet, Hanoi, Vietnam, 100000

[2]*University of Transport Technology*
54 Trieu Khuc, Thanh Xuan, Hanoi, Vietnam, 100000

✉**Corresponding author**

Abstract

The paper presents a dynamic model of the TMM-3M heavy mechanized bridge during the span lowering stage. The model is constructed as a multi-body mechanical system, taking into account the elastic deformation of the cable, rear outriggers, front tires, and front suspension system. It is a mechanical model driven by a cable mechanism. Lagrangian equations of the second kind have been applied to establish a system of differential equations describing the oscillations of the mechanical system and serve as the basis for investigating the dynamics of the span-lowering process. The system of differential equations is solved using numerical methods based on MATLAB simulation software. The study has revealed laws of the displacement, velocity, and acceleration of components within the mechanical system, especially those related to the bridge span depending on the choice of the drive speed of the engine during lowering by operator. The research results show that the lowering time increases from 52 seconds to 104 seconds when the engine speed decreases from 1800 rpm to 900 rpm. The tension force on the cable is surveyed to confirm the safety conditions during the span-lowering process. The study also provides recommendations for selecting appropriate engine speeds to minimize span-lowering time while ensuring the safety conditions of the TMM-3M bridge during the span-lowering process. This research is an important part of a comprehensive study on the working process of the heavy mechanized bridge TMM-3M to make practical improvements, aiming to reduce deployment time, decrease the number of deployment crew members, and increase the automation capability of the equipment.

Keywords: military bridge, dynamic, TMM-3M, cable, engine speed, multi-body system.

DOI: 10.21303/2461-4262.2024.003365

1. Introduction

The heavy mechanized bridge is commonly deployed in military forces worldwide, typically comprising tracked or wheeled chassis carrying bridging equipment. They are used to rapidly deploy temporary bridges for vehicles and personnel to cross obstacles such as rivers, streams, and ravines. Sometimes, they are also utilized to shorten travel distances by creating shortcuts across water obstacles or deep trenches. The heavy mechanized bridges have been researched and manufactured by many countries worldwide for a long time, especially in Russia and developed European countries [1–3].

The TMM-3M bridge (**Fig. 1**) is a type of heavy mechanized bridge with a Kraz255B truck chassis [4–6], where the truck body has been replaced by the bridge span. The TMM-3M bridge, produced by the Soviet Union for a long time, has certain technological limitations compared

to modern developments. The deployment process of the TMM-3M bridge goes through four stages, starting from lifting the lifting frame, opening the bridge span, lowering the bridge span, and finally lowering the intermediate support legs. The lowering of the TMM-3M bridge is carried out after both halves of the bridge span are fully opened, meaning they are in a straightened state. The bridge span is gradually lowered using a cable mechanism. The cable mechanism is driven by the power source, the original IAMZ-238 engine on the Kraz255B vehicle, through a power transmission system. The lowering time of the bridge span depends on the cable release speed. The cable drum rotates fast or slow depending on the engine speed selection, determined by the transmission ratio from the engine to the cable drum under ideal conditions, where the ratio is constant. It can be seen that during the span-lowering process, only the engine operates to drive the cable mechanism. The TMM-3M bridge is considered to operate reasonably when the lowering time is short while still ensuring conditions including vehicle stability, safety conditions regarding the limit of dynamic cable tension, safety conditions regarding the relationship between the inertial moment and static moment of the bridge span compared to the braking moment to ensure the bridge span can be stopped at any time during the span lowering process.

Fig. 1. The heavy mechanized bridge TMM-3M [4]

Due to the specialized nature of heavy mechanized bridges, primarily used in the military, scientific publications on heavy mechanized bridges in general, and the TMM-3 M bridge in particular, are still very limited. Broad publications on heavy mechanized bridges mainly consist of descriptions of structures, rational structures, and the application of 3D software for strength calculations, without computational and theoretical research [7–12]. Publications on the TMM-3M bridge are also very few. In [13], a 2 DOFs model of the lowering and recovery process of the TMM-3M bridge, including the elastic deformation of the cable, was mentioned but without considering the viscous damping coefficient as presented by the authors. However, too many assumptions lead to errors. In [14], the authors conducted direct studies on the TMM-3M bridge but only stopped at examining the first stage, which is the lifting stage driven by a hydraulic system, which is different from the span lowering process where the bridge span is driven by a cable mechanism.

When studying the working process of the cable mechanism in the span lowering process of the TMM-3M bridge, let's find similar characteristics in terms of structure and operation mechanism to that of the cable crane wheel. The elastic deformation of the cable in mechanical systems and the oscillation of wheeled chassis have also been considered in many published studies. In [15, 16], L. A. Tuan and colleagues studied an overall model of the crawler crane, where the elastic deformation of the cable was considered, including both the elasticity and damping coefficient. A similar study on the wheeled crane was conducted in [17–19], but the authors did not mention the oscillation of the wheeled chassis in these studies. Regarding the oscillation of the wheeled chassis, in studies [20–22], the authors built a model of the suspension system on trucks and trailers, providing results of displacement, velocity, and acceleration during the vehicle movement process. This differs from the span-lowering process of the TMM-3M bridge, as the wheeled chassis remains stationary during the span-lowering process.

The study of the dynamics of the TMM-3M bridge during the span-lowering process to investigate and identify the optimal working mode is essential and practical, especially in combat scenarios, where minimizing the lowering time holds significant value.

2. Materials and methods

2. 1. System description

Characteristics of the span-lowering process include the Kraz255B chassis standing still in place. The torque from the engine is transmitted to the cable drum through a power transmission system consisting of a clutch, gearbox, transfer case, and shafts with constant overall transmission ratios. It is assumed that during the span-lowering process, the TMM-3M bridge stands on an absolutely rigid foundation with no horizontal tilt, vertical slope, wind load, or friction in the joints. Apart from the components considered elastic, such as the cable, front bridge, front tires, and rear outriggers, all other components are assumed to be absolutely rigid, with their centroid positioned at their center of gravity.

The dynamic model of the TMM-3M bridge during the span lowering stage is a flat model described as shown in **Fig. 2**. The entire system is placed in the fixed coordinate system Ox_0y_0. Let's use symbols to describe the dynamic parameters of the system as follows: m_1, m_2, m_3, m_b represent the masses of the front axle, chassis, lifting frame, and bridge span, respectively; G_1, G_2, G_3, G_b are the centroids of m_1, m_2, m_3, m_b; H_1, H_2 are the initial heights of m_1, m_2 relative to the ground; J_2, J_3, J_b, J_t are the inertial moments of the chassis, lifting frame, bridge span, and cable drum around their respective axes of rotation; k_{ft}, k_{fs}, k_{ro}, k_c represent the stiffness of the front tires, front suspension, rear outriggers, and cable; b_{ft}, b_{fs}, b_{ro}, b_c represent the damping coefficients of the front tires, front suspension, rear outriggers, and cable. In addition to the dimensions described in **Fig. 2**, the symbols describing the remaining geometric dimensions are represented as follows, noting that G_2L always has a longitudinal direction along the chassis:

$$l_1 = G_2F;\ l_2 = G_2G_3;\ l_3 = G_2H;\ l_4 = NF;\ l_5 = FG_b;\ l_6 = FH,$$

$$\gamma_1 = \angle FG_2L;\ \gamma_2 = \angle G_3G_2L;\ \gamma_3 = \angle HG_2L;\ \gamma_5 = \angle NFG_b;\ \gamma_6 = \angle HFG_2.$$

One additional point to note about this system is that, during the actual span-lowering process, the driver keeps the accelerator pressed to maintain a constant engine speed and disengages the clutch to transmit motion from the engine to the cable drum.

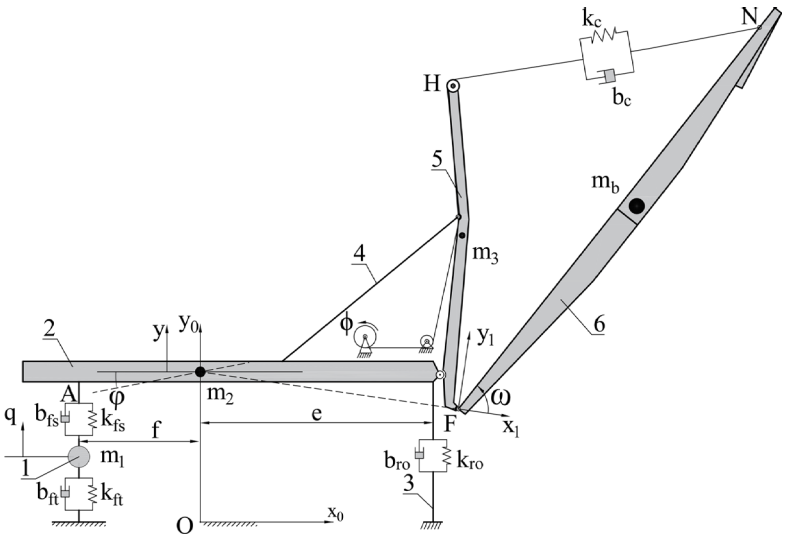

Fig. 2. Dynamic model of the TMM-3M bridge during the span lowering stage:
1 – front axle; 2 – chassis; 3 – rear outriggers; 4 – linkages;
5 – lifting frame; 6 – bridge span

2. 2. Motion equations

2. 2. 1. Generalized coordinates

Generalized coordinates have been assumed, which vector (**Fig. 2**) has the form:

$$\begin{bmatrix} q & y & \varphi & \omega & \phi \end{bmatrix}^T, \tag{1}$$

where $q(m)$ – vertical displacement of the unsprung mass of the front axle; $y(m)$ – vertical displacement of the center of mass of the chassis; $\varphi(rad)$ – pitch angle of the chassis; $\omega(rad)$ – angular displacement of the span; $\phi(rad)$ – rotational angle of the cable drum.

2. 2. 2. The kinetic energy, the potential energy and the total dissipative energy of the system

The kinetic energy of the system is determined by the expression:

$$T = \frac{1}{2}m_1\dot{q}^2 + \frac{1}{2}m_2\dot{y}^2 + \frac{1}{2}(J_2 + J_3)\dot{\varphi}^2 + \frac{1}{2}J_b\dot{\omega}^2 + \frac{1}{2}J_t\dot{\phi}^2 + \frac{1}{2}m_3\left(l_2^2\dot{\varphi}^2 + \dot{y}^2 + 2l_2\cos(\varphi+\gamma_2)\dot{\varphi}\dot{h}\right) +$$
$$+\frac{1}{2}m_b\begin{pmatrix} l_1^2\dot{\varphi}^2 + \dot{y}^2 + l_5^2(\dot{\varphi}+\dot{\omega})^2 + 2l_1l_5\cos(\omega-\gamma_5)(\dot{\varphi}+\dot{\omega})\dot{\varphi} + \\ +2l_1\cos(\varphi-\gamma_1)\dot{\varphi}\dot{h} + 2l_5\cos(\varphi+\omega-\gamma_1-\gamma_5)(\dot{\varphi}+\dot{\omega})\dot{h} \end{pmatrix}. \tag{2}$$

The total potential energy of the system is determined by the expression:

$$\Pi = m_1g(q+H_1) + m_2g(y+H_2) + m_3g\begin{pmatrix} y+H_2+ \\ +l_2\sin(\varphi+\gamma_2) \end{pmatrix} + m_bg\begin{pmatrix} y+H_2+l_1\sin(\varphi-\gamma_1)+ \\ +l_5\sin(\varphi+\omega-\gamma_1-\gamma_5) \end{pmatrix} +$$
$$+\frac{1}{2}k_c\Delta l^2 + \frac{1}{2}k_{fs}(y-q-f\varphi)^2 + \frac{1}{2}k_{ft}q^2 + \frac{1}{2}k_{ro}(y+e\varphi)^2. \tag{3}$$

The total dissipative energy of the system is determined by the following expression:

$$\Phi = \frac{1}{2}b_{fs}(\dot{y}-\dot{q}-f\dot{\varphi})^2 + \frac{1}{2}b_{ft}\dot{q}^2 + \frac{1}{2}b_{ro}(\dot{y}+e\dot{\varphi})^2 + \frac{1}{2}b_c(\dot{\Delta l})^2. \tag{4}$$

In expression (3), Δl represents the total deformation of the cable, including static deformation Δl_s and dynamic deformation Δl_d, and is determined by the expression:

$$\Delta l = L\left(1 + \frac{m_bgl_5}{k_cl_6l_4}\frac{\cos(\varphi+\omega-\gamma_1-\gamma_5)}{\sin(\omega+\gamma_6)}\right) - R_t\phi + R_t\phi_0 - L_0, \tag{5}$$

L and L_0 represent the length of the HN cable at any given time and at the start of the survey, respectively. There is:

$$L = \sqrt{l_6^2 + l_4^2 + 2l_4l_6\cos(\omega+\gamma_6)},$$

$$L_0 = \sqrt{l_6^2 + l_4^2 + 2l_4l_6\cos(\omega_0+\gamma_6)}. \tag{6}$$

The expression defining $\dot{\Delta l}$ in expression (4) is:

$$\dot{\Delta l} = \frac{-l_4l_6\sin(\omega+\gamma_6)\dot{\omega}}{L}\left(1 + \frac{m_bgl_5}{k_cl_6l_4}\frac{\cos(\varphi+\omega-\gamma_1-\gamma_5)}{\sin(\omega+\gamma_6)}\right),$$
$$+\frac{m_bgl_5L}{k_cl_6l_4}\frac{\begin{Bmatrix} -\sin(\varphi+\omega-\gamma_1-\gamma_5)\sin(\omega+\gamma_6)\dot{\varphi} \\ -\dot{\omega}\cos(\varphi-\gamma_1-\gamma_5-\gamma_6)\dot{\omega} \end{Bmatrix}}{\sin^2(\omega+\gamma_6)} - R_t\dot{\phi}. \tag{7}$$

2. 2. 3. Generalized forces

During the lowering process, the brake band on the cable drum is typically kept in a fixed, non-adjustable state to ensure safety. To drive the cable drum, torque from the engine is transmitted and converted into cable drum torque. This torque must exceed the difference between the brake torque and the torque caused by the changing load on the cable drum. Let M_n denote the torque induced by external forces acting on the cable drum. The feasible displacement work of the external forces acting on the system is:

$$\delta A = M_n \delta\phi. \tag{8}$$

2. 2. 4. The system of differential equations

In practice, when lowering the TMM-3M bridge, the driver performs the following steps sequentially: depress the accelerator pedal to increase the engine speed to a certain value and maintain that speed, shift the gear lever to reverse, and finally release the clutch to transmit torque from the engine to the cable drum. Thus, the speed of the cable drum can be considered constant. The system has four degrees of freedom. Apply the Lagrange's second kind equation to formulate the system of differential equations describing the oscillations of the system in the form [14, 17]:

$$\frac{d}{dt}\left(\frac{T}{\partial\dot{q}_i}\right)-\frac{\partial T}{\partial q_i}+\frac{\partial\Pi}{\partial q_i}+\frac{\partial\Phi}{\partial\dot{q}_i}=Q_i\left(i=1\div 4\right). \tag{9}$$

Let $\mathbf{q}=\left[q \quad y \quad \varphi \quad \omega\right]^T$; $\dot{\mathbf{q}}=\left[\dot{q} \quad \dot{y} \quad \dot{\varphi} \quad \dot{\omega}\right]^T$; $\ddot{\mathbf{q}}=\left[\ddot{q} \quad \ddot{y} \quad \ddot{\varphi} \quad \ddot{\omega}\right]^T$.

Substituting the expressions for kinetic energy, potential energy, and dissipative functions into equation (9), let's obtain the system of differential equations describing the oscillations of the system as follows:

$$M\ddot{\mathbf{q}}+C\dot{\mathbf{q}}+K\mathbf{q}+G=Q. \tag{10}$$

The matrix $M=\left[m_{ij}\right],\left(i,j=\overline{1,4}\right)$ in equation (10) is determined as follows:

$$m_{11}=m_1;\ m_{12}=m_{21}=0;\ m_{13}=m_{31}=0;\ m_{14}=m_{41}=0,$$

$$m_{22}=m_2+m_3+m_b;\ m_{24}=m_{42}=m_b l_5\cos\left(\varphi+\omega-\gamma_1-\gamma_5\right),$$

$$m_{23}=m_3 l_2\cos\left(\varphi+\gamma_2\right)+m_b\left(l_1\cos\left(\varphi-\gamma_1\right)+l_5\cos\left(\varphi+\omega-\gamma_1-\gamma_5\right)\right),$$

$$m_{32}=m_{23};\ m_{33}=J_2+J_3+m_3 l_2^2+m_b\left(l_1^2+l_5^2+2l_1 l_5\cos\left(\omega-\gamma_5\right)\right),$$

$$m_{34}=m_{43}=m_b\left(l_5^2+l_1 l_5\cos\left(\omega-\gamma_5\right)\right);\ m_{44}=J_b+m_b l_5^2. \tag{11}$$

The matrix $C=\left[c_{ij}\right],\left(i,j=\overline{1,4}\right)$ in equation (10) is determined as follows:

$$c_{11}=b_{fs}+b_{ft};\ c_{12}=c_{21}=-b_{fs};\ c_{13}=c_{31}=b_{fs}f;\ c_{14}=c_{41}=0,$$

$$c_{22}=b_{fs}+b_{ro};\ c_{24}=-m_b l_5\sin\left(\varphi+\omega-\gamma_1-\gamma_5\right)\left(2\dot{\varphi}+\dot{\omega}\right),$$

$$c_{23}=b_{ro}e-b_{fs}f-\left\{m_3 l_2\sin\left(\varphi+\gamma_2\right)+m_b\begin{pmatrix}l_1\sin\left(\varphi-\gamma_1\right)+\\+l_5\sin\left(\varphi+\omega-\gamma_1-\gamma_5\right)\end{pmatrix}\right\}\dot{\varphi},$$

$$c_{32}=b_{ro}e-b_{fs}f;\ c_{33}=b_{fs}f^2+b_{ro}e^2;\ c_{34}=-m_b l_1 l_5\sin\left(\omega-\gamma_5\right)\left(2\dot{\varphi}+\dot{\omega}\right),$$

$$c_{42}=0;\ c_{43}=m_b l_1 l_5\sin\left(\psi-\gamma_5\right)\dot{\varphi};\ c_{44}=0. \tag{12}$$

The matrix $K=\left[k_{ij}\right],\left(i,j=\overline{1,4}\right)$ in equation (10) is determined as follows:

$$k_{11}=k_{fs}+k_{ft};\ k_{12}=k_{21}=-k_{fs};\ k_{13}=k_{31}=k_{fs}f;\ k_{14}=k_{41}=0;\ k_{22}=k_{fs}+k_{ro},$$

$$k_{23}=k_{32}=-k_{fs}f+k_{ro}e;\ k_{24}=k_{42}=0;\ k_{33}=k_{fs}f^2+k_{ro}e^2;\ k_{34}=k_{43}=0;\ k_{44}=0. \quad (13)$$

The matrix $G=\left[g_1 \quad g_2 \quad g_3 \quad g_4\right]^T$ in equation (10) is determined as follows:

$$g_1=m_1g;\ g_2=\left(m_2+m_3+m_b\right)g;\ g_4=m_bgl_5\cos\left(\varphi+\omega-\gamma_1-\gamma_5\right),$$

$$g_3=m_3gl_2\cos\left(\varphi+\gamma_2\right)+m_bg\left(l_1\cos\left(\varphi-\gamma_1\right)+l_5\cos\left(\varphi+\omega-\gamma_1-\gamma_5\right)\right). \quad (14)$$

The matrix $Q=\left[0 \quad 0 \quad Q_3 \quad Q_4\right]^T$ in equation (10) is determined as follows:

$$Q_3=-k_c\Delta l\left(\Delta l\right)'_{\varphi}-b_c\dot{\Delta}l\left(\dot{\Delta}l\right)'_{(\dot{\varphi})};\ Q_4=-k_c\Delta l\left(\Delta l\right)'_{\omega}-b_c\dot{\Delta}l\left(\dot{\Delta}l\right)'_{(\dot{\omega})}. \quad (15)$$

In expression (15), $\left(\Delta l\right)'_{\varphi},\left(\dot{\Delta}l\right)'_{(\dot{\varphi})},\left(\Delta l\right)'_{\omega},\left(\dot{\Delta}l\right)'_{(\dot{\omega})}$ are defined as follows:

$$\left(\Delta l\right)'_{\varphi}=\left(\dot{\Delta}l\right)'_{(\dot{\varphi})}=\frac{-m_bgl_5L\sin\left(\varphi+\omega-\gamma_1-\gamma_5\right)}{k_cl_6l_4\sin\left(\omega+\gamma_6\right)},$$

$$\left(\Delta l\right)'_{\omega}=\left(\dot{\Delta}l\right)'_{(\dot{\omega})}=\frac{m_bgl_5L}{k_cl_6l_4}\frac{\cos\left(\varphi-\gamma_1-\gamma_5-\gamma_6\right)}{\sin^2\left(\omega+\gamma_6\right)}+$$
$$+\frac{-l_4l_6\sin\left(\omega+\gamma_6\right)}{L}\left(1+\frac{m_bgl_5}{k_cl_6l_4}\frac{\cos\left(\varphi+\omega-\gamma_1-\gamma_5\right)}{\sin\left(\omega+\gamma_6\right)}\right). \quad (16)$$

The Matlab software application is used to solve a system of differential equations (10) with given initial conditions is:

$$\left[q_0 \quad y_0 \quad \varphi_0 \quad \omega_0\right]^T=\left[q_0 \quad y_0 \quad \varphi_0 \quad 1.5\right]^T,$$

$$\left[\dot{q}_0 \quad \dot{y}_0 \quad \dot{\varphi}_0 \quad \dot{\omega}_0\right]^T=\left[0 \quad 0 \quad 0 \quad 0\right]^T.$$

The table of input parameters to solve (10) is in **Table 1**.

Table 1

Factors and value (all parameters are in SI-units)

Parameter	Value	Parameter	Value	Parameter	Value
e	2.24	b_{ro}	500	γ_6	1.6246
f	5.62	b_c	500	m_1	910
l_1	8.51	k_{ft}	800000	m_2	8390
l_2	7.46	k_{fs}	295000	m_3	950
l_3	9.21	k_{ro}	10^8	m_b	5600
l_4	9.5	k_c	2300000	J_2	39252
l_5	5.25	γ_1	0.0872	J_3	13912
l_6	7.0	γ_2	0.543	J_b	38587
b_{ft}	500	γ_3	0.7306	R_t	0.12
b_{fs}	24000	γ_5	0.07	ϕ_0	0

2. 2. 5. The cable tension force

During the process of lowering the bridge span, safety is always a concern due to the dynamic loading that occurs. The dynamic tension force generated during the lowering process must always be kept below the allowable value of 162000 N. The dynamic tension force F_d appearing during the lowering process is determined by the expression:

$$F_d = \frac{m_b g l_5 L \cos(\varphi + \omega - \gamma_1 - \gamma_5)}{l_6 l_4 \sin(\omega + \gamma_6)} + k_c (L - L_0 - R_t \phi) + b_c (\dot{\Delta} l). \quad (17)$$

3. Results and discussion

3. 1. The span-lowering time according to the engine speed

Let's survey the influence of selecting the engine speed on the dynamics of the TMM-3M bridge during the span-lowering process. The survey investigates the effect of engine speed on the angular ω of the bridge during span-lowering in 10 cases, ranging from 900 rpm to 1800 rpm. The results are shown in **Fig. 3**, with **Fig. 3, *b*** being an excerpt to illustrate the variation of ω over time more clearly.

The oscillation of A exhibits a decaying pattern. The damping time of the oscillation is approximately 15 seconds. This also indicates that at the beginning of the span-lowering process, the bridge span will experience the most intense oscillations, gradually stabilizing as the curve representing the angular velocity ω becomes smoother. In a separate survey with the engine speed set at 1400 rpm, let's obtain the graphs of angular velocity and angular acceleration of the bridge span, as depicted in **Fig. 4**.

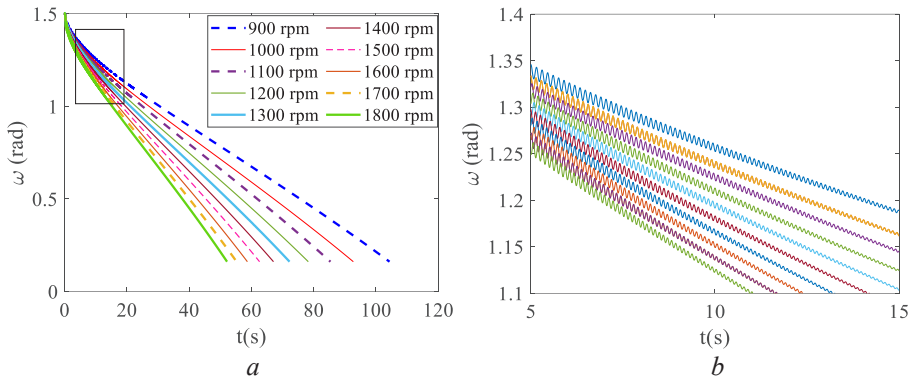

Fig. 3. The graph of the bridge span's angular ω: *a* – the original graph; *b* – zoomed-in graph section

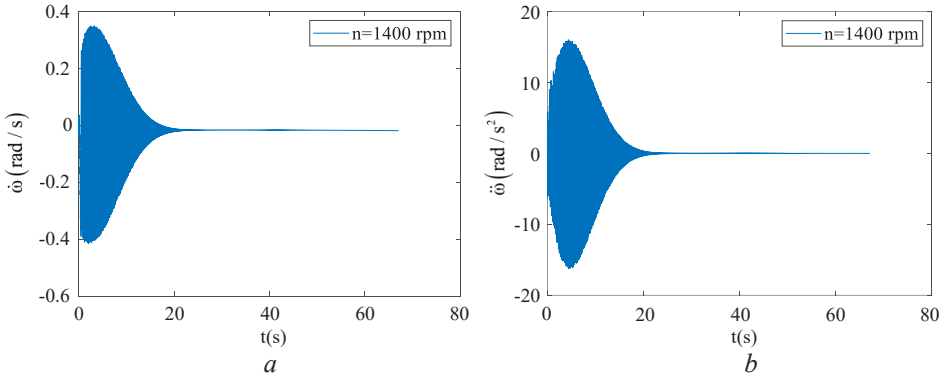

Fig. 4. Vibration of the bridge span: *a* – angular velocity; *b* – angular acceleration

From the graph in **Fig. 4, *a***, let's observe that as the engine speed increases, the time taken to complete the span-lowering stage decreases. This reduction in lowering time is more pronounced at lower engine speeds. At engine speeds ranging from 900 rpm to 1300 rpm, increasing the engine speed by an additional 100 rpm results in a significant decrease in lowering time, ranging from 7 to 12 seconds. However, when increasing the engine speed by an additional 100 rpm within

the range of speeds from 1400 rpm to 1800 rpm, the lowering time only decreases by 3 to 5 seconds. The relationship between the lowering time of the bridge and the engine speed, corresponding to the 10 surveyed cases, is depicted in **Fig. 5**.

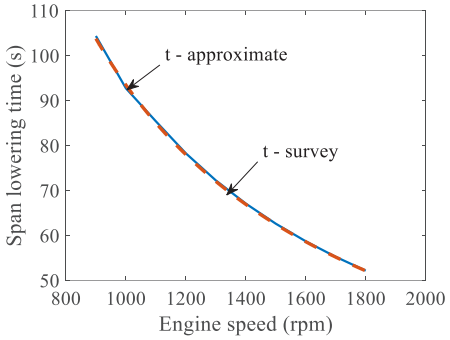

Fig. 5. The span-lowering time *t*

Using the interpolation method, after conducting 10 surveyed cases of lowering time according to engine speed, it is approximately representing the dependency of the lowering time $t(s)$ on the engine speed $n(rpm)$ according to the exponential function law as follows:

$$t = 89041 \times n^{-0.993}. \tag{18}$$

(18) helps approximately determine the span-lowering time corresponding to the engine speed at any given time. It is possible to determine that the span-lowering time at an engine speed of 1800 rpm is approximately 52 seconds, and the span-lowering time at an engine speed of 900 rpm is approximately 104 seconds.

3. 2. The oscillation of the vehicle chassis

Let's survey the oscillation of the vehicle chassis in the case of an engine speed of 1400 rpm. The displacement and velocity of m_1 and m_2, the angular displacement and pitch angle of the vehicle chassis, are depicted in **Fig. 6**.

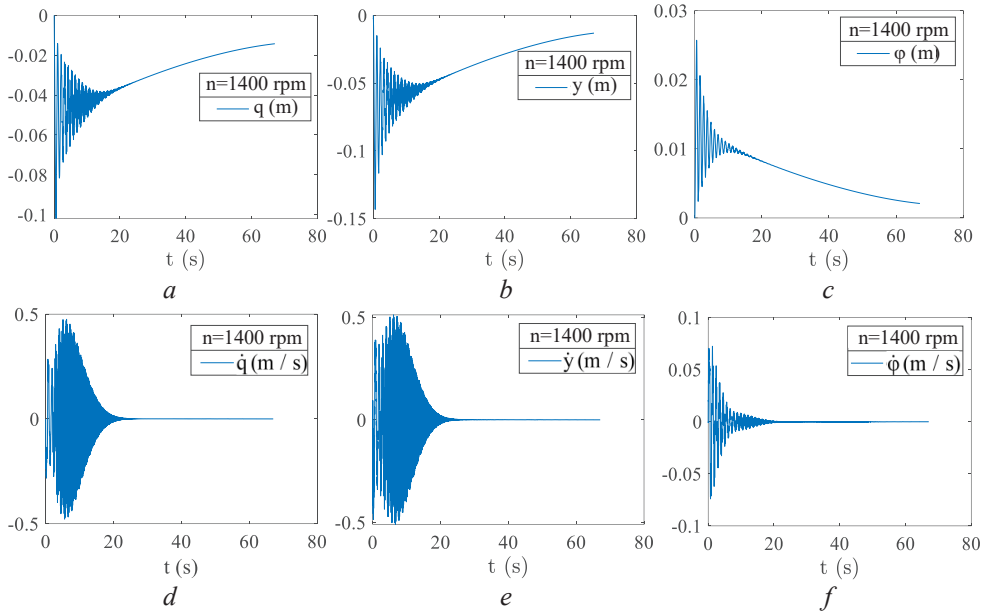

Fig. 6. Vibration of the base vehicle: *a* – front axle displacement; *b* – chassis displacement; *c* – chassis roll angle; *d* – front axle velocity; *e* – chassis velocity; *f* – angular velocity of the chassis

The displacement and velocity laws shown in **Fig. 7** demonstrate the coherence of the oscillation laws between the vehicle chassis and the bridge span. At the beginning of the span-lowering phase, it is possible to observe that the bridge span experiences the most intense oscillations, coinciding with the period when the vehicle chassis exhibits the strongest oscillations. Subsequently, the oscillations of the vehicle chassis become smoother and gradually diminish. The graph in **Fig. 6** illustrates that as the lowering phase approaches its end, the center of mass of the bridge span moves further away from the axis of rotation. Therefore, both m_1 and m_2 tend to elevate gradually relative to the ground.

The survey results from the remaining 9 cases of engine speed indicate that the laws governing q, y, ϕ, and their corresponding velocities are very similar and akin to the case of an engine speed of 1400 rpm.

3. 3. The investigation of tension forces

The span-lowering stage is critical because of the significant load on the bridge span and the oscillations of both the bridge span and the vehicle chassis, resulting in dynamic loads. To assess the allowable tension conditions for the cables during the span-lowering process, it is possible to conduct a survey of the static tension force and the dynamic tension force appearing on the cables during the span-lowering stage.

The survey results of the dynamic tension force F_d in 10 cases of engine speeds ranging from 900 rpm to 1800 rpm are depicted in **Fig. 7**. At the initial stage of the span-lowering process, the strong oscillation of the bridge span leads to a dynamic tension force with a large oscillation amplitude, as shown in **Fig. 7, *b***, which is an enlarged portion of the graph from **Fig. 7, *a***.

Surveying two cases of engine speeds, 1400 rpm and 1500 rpm, to explore the correlation between static tension force F_s and dynamic tension force F_d during the span-lowering phase, let's obtain the results depicted in **Fig. 8**.

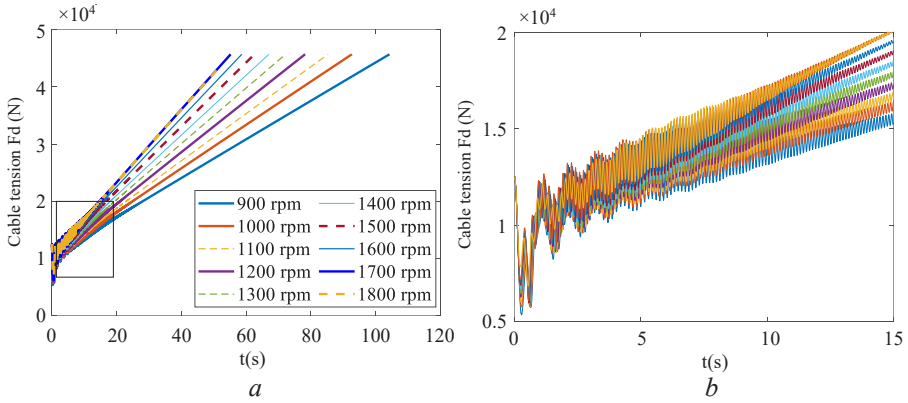

Fig. 7. The dynamic tension force: *a* – the original graph; *b* – zoomed-in graph section

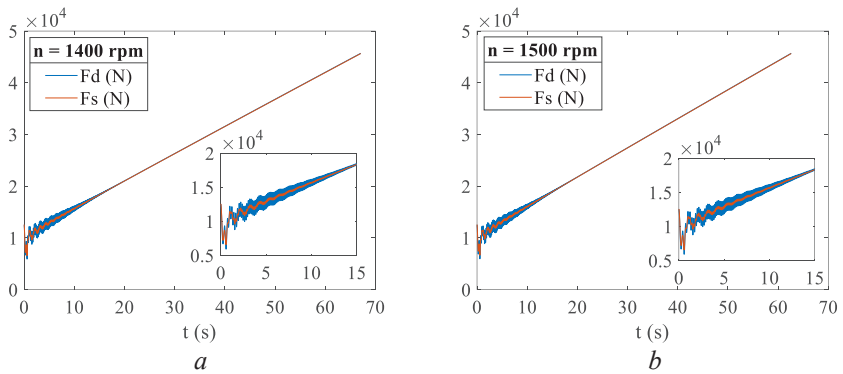

Fig. 8. The correlation between static tension force and dynamic tension force: *a* – when $n = 1400$ rpm; *b* – when $n = 1500$ rpm

From the graph in **Fig. 8**, it is possible to observe that the dynamic tension force and the static tension force vary by the same law. During the first 15 seconds of the span-lowering phase, this variation is most pronounced, as indicated by a larger oscillation amplitude compared to the rest of the stage. From **Fig. 7, 8**, it is possible to notice that the tension force tends to increase gradually over the span-lowering time and reaches its maximum value at the end of the phase, approximately 46000 N, which is significantly lower than the cable's withstand limit of 162000 N.

3. 4. Limitations of the research and directions for its further development

The survey results mentioned above are associated with the dynamic model of the TMM-3M bridge during the span-lowering stage under the assumption of neglecting the effects of wind load and characteristics of the ground, such as slope and elasticity. Although the presented results are reasonable, for a more in-depth consideration of the TMM-3M bridge-span-lowering process, it is essential to take into account the factors that have been neglected. This is an issue that should continue to be investigated in the future. The deployment process of the TMM-3M bridge is a complex process consisting of multiple stages. Linking these stages to gain an overall understanding of the dynamics of the TMM-3M bridge throughout the entire deployment process is also necessary.

4. Conclusions

The article presents the dynamic model of the TMM-3M heavy mechanized bridge during the span-lowering phase, with the assumption of neglecting the effects of wind load and ground slope. The results of the article have indicated an approximate law regarding the lowering time dependence on the engine speed. The lowering time decreases by 50 seconds when increasing the engine speed from 900 rpm to 1800 rpm. The survey results also demonstrate the variation law of tension forces on the cables during the lowering process. The maximum tension force observed in the surveyed cases remains within the allowable limit. This study plays an important role in the comprehensive research of the working process of the TMM-3M bridge, aiming to continue improving the structures and rational drive systems.

Conflict of interest

The authors declare that they have no conflict of interest in relation to this research, whether financial, personal, authorship or otherwise, that could affect the research and its results presented in this paper.

Financing

The study was performed without financial support.

Data availability

Manuscript has no associated data.

Use of artificial intelligence

The authors confirm that they did not use artificial intelligence technologies when creating the current work.

Acknowledgements

The authors would like to thank the Le Quy Don Technical University for giving me the opportunity to conduct this research.

References

[1] Russell, B. R., Thrall, A. P. (2013). Portable and Rapidly Deployable Bridges: Historical Perspective and Recent Technology Developments. Journal of Bridge Engineering, 18 (10), 1074–1085. https://doi.org/10.1061/(asce)be.1943-5592.0000454

[2] Kim, Y. J., Tanovic, R., Wight, R. G. (2010). Load Configuration and Lateral Distribution of NATO Wheeled Military Trucks for Steel I-Girder Bridges. Journal of Bridge Engineering, 15 (6), 740–748. https://doi.org/10.1061/(asce)be.1943-5592.0000113

[3] Szelka, J., Wysoczański, A. (2022). Modern structures of military logistic bridges. Open Engineering, 12 (1), 1106–1112. https://doi.org/10.1515/eng-2022-0391
[4] Nemzeti Közszolgálati Egyetem. Available at: https://kvi.uni-nke.hu
[5] KrAZ-255. Available at: https://en.wikipedia.org/wiki/KrAZ-255
[6] KRAZ-255. Available at: https://mortarinvestments.eu/catalog/item/kraz-255
[7] Han, J., Zhu, P., Tao, L., Chen, G., Zhang, S., Yang, X. (2019). An optimum design method for a new deployable mechanism in scissors bridge. Proceedings of the Institution of Mechanical Engineers, Part C: Journal of Mechanical Engineering Science, 233 (19-20), 6953–6966. https://doi.org/10.1177/0954406219869046
[8] Abdi, F., Qian, Z., Mosallam, A., Iyer, R., Wang, J.-J., Logan, T. (2006). Composite army bridges under fatigue cyclic loading. Structure and Infrastructure Engineering, 2 (1), 63–73. https://doi.org/10.1080/15732470500254691
[9] Kalangi, C., Sidagam, Y. (2016). Design and Analysis of Armored Vehicle Launched Bridge (AVLB) for Static Loads. IJSRD – International Journal for Scientific Research & Development, 4 (10), 9–18. Available at: https://www.ijsrd.com/articles/IJSRD-V4I100023.pdf
[10] Osman, A. M. A. (2016). Design optimization of composite deployable bridge systems using hybrid meta-heuristic methods for rapid post-disaster mobility. Concordia University. Available at: https://core.ac.uk/download/pdf/211519275.pdf
[11] Norazman Mohamad Nor (2011). Static analysis and design of sandwiched composite long-span portable beam. African Journal Of Business Management, 6 (27). https://doi.org/10.5897/ijps11.129
[12] Kuczmarski, F., Zelkowski, J., Gontarczyk, M. (2005). Formation of Geometrical Structure of Manipulator for Mechanized Bridge. Proceedings of the International Symposium on Automation and Robotics in Construction (IAARC). https://doi.org/10.22260/isarc2005/0081
[13] Quang, L. H. (2017). Research to determine the dynamic parameters of the folding mechanism of the TMM-3M brigde. Military Technical Academy, Ha Noi.
[14] Thang, T. D., Le, D. V., Chu, D. V. (2024). Research on the dynamics of a heavy mechanized bridge in the deployment phase of the lifting frame. EUREKA: Physics and Engineering, 1, 116–126. https://doi.org/10.21303/2461-4262.2024.003220
[15] Tuan, L. A., Lee, S.-G. (2018). Modeling and advanced sliding mode controls of crawler cranes considering wire rope elasticity and complicated operations. Mechanical Systems and Signal Processing, 103, 250–263. https://doi.org/10.1016/j.ymssp.2017.09.045
[16] Tuan, L. A. (2019). Fractional-order fast terminal back-stepping sliding mode control of crawler cranes. Mechanism and Machine Theory, 137, 297–314. https://doi.org/10.1016/j.mechmachtheory.2019.03.027
[17] Duong, L. V., Tuan, L. A. (2022). Modeling and observer-based robust controllers for telescopic truck cranes. Mechanism and Machine Theory, 173, 104869. https://doi.org/10.1016/j.mechmachtheory.2022.104869
[18] Ngo, Q. H., Hong, K.-S. (2012). Adaptive sliding mode control of container cranes. IET Control Theory & Applications, 6 (5), 662. https://doi.org/10.1049/iet-cta.2010.0764
[19] Mijailović, R. (2012). Modelling the dynamic behaviour of the truck-crane. Transport, 26(4), 410–417. https://doi.org/10.3846/16484142.2011.642946
[20] Jiang, J., Li, P., Chen, Y., Li, Q. (2021). Ride comfort of heavy vehicles based on key response characteristics of multibody dynamics. Proceedings of the Institution of Mechanical Engineers, Part K: Journal of Multi-Body Dynamics, 235 (4), 553–567. https://doi.org/10.1177/14644193211039918
[21] Nakhaie-Jazar, G., Esmailzadeh, E., Mehri, B. (1997). Vibration of road vehicles with non linear suspensions. International Journal of Engineering, 10 (4), 209–218.
[22] Tuan, N. V., Quynh, L. V., Thao, V. T. P., Duy, L. Q. (2020). Optimal design parameters of air suspension systems for semi-trailer truck. Part 1: modeling and algorithm. Vibroengineering PROCEDIA, 33, 72–77. https://doi.org/10.21595/vp.2020.21562

Received date 05.02.2024
Accepted date 05.04.2024
Published date 22.07.2024

How to cite: *Duong, L. V., Thang, T. D., Quyen, D. M., Dat, C. V. (2024). Studying the influence of engine speed on the entire process of span-lowering of the heavy mechanized bridge. EUREKA: Physics and Engineering, 4, 79–89. https://doi.org/10.21303/2461-4262.2024.003365*